Surface Science 639 (2015) 75–79

Contents lists available at ScienceDirect

Surface Science

journal homepage: www.elsevier.com/locate/susc

Influence of the projectile charge state on electron emission spectra from a Cu(111) surface

C.D. Archubi [a,*], V.M. Silkin [b,c], M.S. Gravielle [a]

[a] Instituto de Astronomía y Física del Espacio (IAFE, CONICET-UBA), Casilla de Correo 67, Sucursal 28, C1428EGA Buenos Aires, Argentina
[b] Depto. de Física de Materiales, Facultad de Ciencias Químicas, Universidad del País Vasco, Apdo. 1072, 20080 San Sebastián, Spain
[c] IKERBASQUE, Basque Foundation for Science, 48011 Bilbao, Spain

ARTICLE INFO

Article history:
Received 12 December 2014
Accepted 28 April 2015
Available online 5 May 2015

Keywords:
Electron emission spectra
Surface
Ions collisions

ABSTRACT

Double differential electron emission distributions produced by grazing impact of fast dressed ions on a Cu(111) surface are investigated focusing on the effects of the electronic band structure. The process is described within the Band-Structure-Based approximation, which is a perturbative method that includes an accurate representation of the electron–surface interaction, incorporating information of the electronic band structure of the solid. Differences in the behavior of the emission spectra for He^{+q}, Li^{+q}, Be^{+q} and C^{+q} projectiles with different charge states q are explained by the combined effect of the projectile trajectory and the projectile charge distribution.

1. Introduction

The impact of multicharged ions on solid surfaces has become of great interest in the last two decades [1, 2]. In grazing collisions with metal surfaces, the degree of ionization of the projectile depends on its velocity [3, 4] and the characteristics of the surface [5–10], affecting the stopping and the electron emission probability [11, 12]. For intermediate energies, ionic projectiles grazingly impinging on solid surfaces move parallel to the surface, in the selvage region, with different charge states depending on complex electron capture and loss mechanisms [13–15]. Therefore, these different electronic configurations of the incident particles are expected to have an effect upon the angular and energy distributions of emitted electrons.

On the other hand, recent experimental and theoretical works showed that the band structure of different metal surfaces plays an important role in projectile induced processes [8,16–21,23–25]. In particular, in previous articles [26, 27] we found that the electron emission distributions produced by grazing incidence of protons on Be(0001), Cu(111), Ag(111), Au(111) and Mg(0001) surfaces present prominent signatures of the surface band structure, with pronounced shoulders due to the contribution of partially occupied surface electronic states (SESs). Thus, the aim of this work is to investigate to what extent such structures are affected by the charge state of the projectile.

To describe the electron emission process from the valence band we employ the Band-Structure-Based (BSB) approximation, which is derived within the framework of the binary collisional formalism by including a precise representation of the surface interaction. For every individual electronic excitation, the BSB transition matrix is evaluated making use of the electronic states corresponding to the potential model of Ref. [28]. This potential incorporates effects of the band structure of the metal, properly reproducing the projected energy gap and the energies of the surface and first image states [23–31]. The interaction with projectile electrons is included within the BSB method by means of an effective projectile charge that depends on the transferred momentum, while the dynamic response of the medium to the incident projectile is obtained from the unperturbed electronic wave functions by using the linear response theory.

In this article we study double differential — energy and angle-resolved - electron spectra produced by different ions — He^{+q}, Li^{+q}, Be^{+q} and C^{+q} with different charge states q — grazingly impinging on a Cu (111) surface. We focus on the contribution of partially occupied SESs to the electron emission process, analyzing separately the influence of the projectile trajectory and the projectile charge distribution.

The paper is organized as follows. In Section 2 we summarize the theoretical model, results are presented and discussed in Section 3, and Section 4 contains our conclusions. Atomic units, i.e., $e^2 = \hbar = m_e = 1$, are used unless otherwise stated.

2. Theoretical method

We consider an ionic projectile P, carrying N electrons with it, which impinges grazingly on a metal surface with velocity v. At intermediate and high impact energies, the contribution of the electron loss from the projectile to the electron spectrum becomes relevant in the electron energy region around the convoy peak [32]. But far apart from such energy region, the electron emission is mainly produced by target

* Corresponding author.
E-mail address: archubi@iafe.uba.ar (C.D. Archubi).

http://dx.doi.org/10.1016/j.susc.2015.04.023
0039-6028/

excitations and we can assume that projectile electrons remain frozen in their initial states during the whole collision process.

Within the binary collisional formalism, the transition probability per unit path for the target excitation $i \to f$ reads [34]:

$$P_{if}(Z) = \frac{2\pi}{v_s}\delta(\Delta)|T_{if}|^2, \tag{1}$$

where the initial state i belongs to the electron valence band of the metal, with initial energy E_i below the Fermi level, while the final state f lays in the continuum above the vacuum level, with final energy $E_f \geq 0$. In Eq. (1) Z denotes the projectile distance to the surface, v_s is the component of the projectile velocity parallel to the surface plane, and the Dirac delta function $\delta(\Delta)$ expresses the energy conservation, with

$$\Delta = \mathbf{v}_s \cdot (\mathbf{k}_{fs} - \mathbf{k}_{is}) - (E_f - E_i), \tag{2}$$

and $\mathbf{k}_{is}$ ($\mathbf{k}_{fs}$) the initial (final) electron momentum parallel to the surface.

The T-matrix element, T_{if}, is evaluated here within a first-order perturbation theory, reading:

$$T_{if} = \langle \Psi_f | V | \Psi_i \rangle, \tag{3}$$

where V denotes the perturbative potential and $\Psi_i(\Psi_f)$ is the initial (final) unperturbed electronic state. By considering projectile electrons as passive ones — which do not participate in the electronic transition — the unperturbed wave function can be expressed as $\Psi_{i(f)} = \Phi_{pass}\Phi_{i(f)}$, where Φ_{pass} represents the electronic wave function corresponding to the projectile passive electrons, while $\Phi_i(\Phi_f)$ is the wave function of the initial (final) unperturbed state corresponding to the active target electron. In this work Φ_{pass} is represented in terms of ionic Hartree–Fock orbitals, as given by Ref. [33], while the wave functions Φ_i and Φ_f are obtained from the BSB model as $\Phi_i = \Phi_{\mathbf{k}_{is},n_i}$ and $\Phi_f = \Phi_{\mathbf{k}_{fs},n_f}$:

$$\Phi_{\mathbf{k}_s,n}(\mathbf{r}) = \frac{1}{2\pi}\exp(i\mathbf{k}_s.\mathbf{r}_s)\phi_n(z), \tag{4}$$

where $\mathbf{r} \equiv (\mathbf{r}_s, z)$ is the position vector of the active electron, with $\mathbf{r}_s$ and z being the components of $\mathbf{r}$ parallel and perpendicular, respectively, to the surface plane. The function $\phi_n(z)$ represents the eigenfunction of the one-dimensional Schrödinger equation associated with the surface potential of Ref. [28] with eigenenergy ε_n. Within a slab geometry, the following representation of $\phi_n(z)$ is used:

$$\phi_n(z) = \frac{1}{\sqrt{L}}\sum_{j=-N}^{N} a_n(j)\exp\left(i\frac{2\pi j}{L}z'\right), \tag{5}$$

where L is a normalization length, $2N+1$ is the number of basis functions, and the coefficients $a_n(j)$ are numerically evaluated. The coordinate $z' = z + d_s$ is measured with respect to the center of the slab, which is placed at a distance d_s from the crystal border.

The potential V involved in Eq. (3) can be expressed as $V = V_{Pe} + V_{ind}$, where V_{Pe} represents the interaction of the projectile with the active electron, while V_{ind} denotes the induced surface potential originated by the rearrangement of the surface electronic density as a consequence of the projectile interaction. The potential V_{Pe} takes into account the screening of the nuclear charge of the projectile Z_P by passive electrons. Its Fourier transform can be expressed as

$$\tilde{V}_{Pe}(\mathbf{Q}) = -\tilde{Z}_P(\mathbf{Q})\sqrt{\frac{2}{\pi}}\frac{1}{Q^2}, \tag{6}$$

where

$$\tilde{Z}_P(\mathbf{Q}) = Z_P - \sum_{j=1}^{N} S_j(\mathbf{Q}) \tag{7}$$

is an effective projectile charge, named here as *structure* charge, which depends on the transferred momentum $\mathbf{Q}$, and the structure factor,

$$S_j(\mathbf{Q}) = \int d\mathbf{r}\, e^{-i\mathbf{Q}.\mathbf{r}}\left|\varphi_j^{pass}(\mathbf{r})\right|^2, \tag{8}$$

with $j = 1,N$, is evaluated by using the electronic states $\varphi_j^{pass}(\mathbf{r})$ corresponding to the N passive electrons carried by the projectile.

By employing the structure charge of Eq. (7) and the wave functions given by Eq. (4) as initial and final electronic states, the BSB transition matrix can be derived from Eq. (3) as:

$$T_{if} = \frac{-1}{(2\pi)^3 L}\sum_{j=-N}^{N} a_{n_f}^*(j)\sum_{j'=-N}^{N} a_{n_i}(j')\tilde{Z}_P(\mathbf{Q}) \times\left\{\frac{2(2\pi)^2\exp\left[-i\,Q_{j,j'}(Z+d_s)\right]}{Q^2} + W_{ind}(\mathbf{Q},Z,\omega)\right\}, \tag{9}$$

where $\mathbf{Q} = \mathbf{Q}_s + Q_{j,j'}\,\hat{z}$ is the partial projectile transferred momentum, with $\mathbf{Q}_s = \mathbf{k}_{fs} - \mathbf{k}_{is}$ the electron momentum transfer parallel to the surface, $Q_{j,j'} = 2\pi(j-j')/L$, and $\hat{z}$ the versor normal to the surface plane, aiming to the vacuum region. In Eq. (9) the function $W_{ind}(\mathbf{Q}, Z, \omega)$ represents the Fourier transform of the induced potential, per unit of projectile charge, which is derived in a consistent way by using the linear response theory [24, 29], with $\omega = \mathbf{Q}_s \cdot v_s$.

The differential transition probability from the valence band to a given final state f with momentum $\mathbf{k}_f$, $dP_{vb}/d\mathbf{k}_f$, is obtained by integrating Eq. (1) along the classical projectile path $Z(X)$, after adding the contributions coming from the different initial states. That is,

$$\frac{dP_{vb}}{d\mathbf{k}_f} = 2\int_0^{+\infty} dX\left[\sum_i \rho_e\Theta(-E_W - E_i)P_{if}(Z(X))\right], \tag{10}$$

where X denotes the coordinate along the incidence direction on the surface plane, $\rho_e = 2$ is associated with the spin states, and the factor 2 takes into account that the ions are specularly reflected at the surface. In Eq. (10) the unitary Heaviside function Θ confines the initial states to those contained within the Fermi sphere, with E_W as the work function. Notice that the Dirac delta function of Eq. (1) restricts the allowed initial momenta with the result that only two different values of k_{is} contribute to every transition $i \to f$.

To determine the classical projectile trajectory we employed the Ziegler–Biersack–Littmark potential [35] plus the BSB induced potential, both evaluated by considering the incident ion as a punctual charge q, with $q = Z_P - N$ the total projectile charge. The BSB induced potential evaluated at the projectile position, $V_{ind}(Z)$, was obtained from $W_{ind}(\mathbf{q}, Z, \omega')$ as

$$V_{ind}(Z) = \frac{q^2}{2(2\pi)^3}\int d\mathbf{p}\, e^{ip_z Z}W_{ind}(\mathbf{p}, Z, \omega'), \tag{11}$$

where $\mathbf{p} = \mathbf{p}_s + p_z\hat{z}$ and $\omega' = \mathbf{p}_s \cdot v_s$. More details of the calculation can be found in Refs. [29, 30].

3. Results

We applied the BSB approximation to investigate electron emission spectra produced by grazing scattering of different ionic projectiles from a Cu(111) surface considering an incidence velocity $v = 2$ a.u. and a glancing incidence angle $\alpha_i = 0.1$ °. This very small angle was chosen to stress band structure contributions to electron emission spectra [27], but it may be nearly reachable with present experimental capabilities [36]. The differential probability of electron emission from the valence band, $dP_{vb}/d\mathbf{k}_f$, was obtained from Eq. (10) following the same procedure as in Ref. [27]. To represent the electronic states of Li^+, Be^+,

Be^{+2}, and C^{+q} we used Hartree–Fock wave functions corresponding to the respective ions [33], while for He^{+}, Li^{+2}, and Be^{+3} we used hydrogenic wave functions.

The Cu(111) surface presents an SES band with a parabolic-like dispersion that is partially occupied, with an energy $\varepsilon_{SES} = -0.44$ eV at the bottom measured with respect to the Fermi level [27]. In a previous article [27] these states were found to leave visible footprints in electron spectra by proton impact, even when electron contributions from the inner-shells of the surface atoms were considered. Therefore, Cu(111) has been used here as a prototype to study the effect of the projectile charge state on the SES structures of electron emission distributions.

With the aim of analyzing the influence of the electronic structure of the projectile on the electron emission distribution, in Fig. 1 we show electron emission probabilities from the valence band, as a function of the electron energy, for different single charged ions: H^{+}, He^{+}, Li^{+}, Be^{+}, and C^{+}. In the figure, results for the ejection angle $\theta_e = 30$ °, measured with respect to the surface in the scattering plane, are displayed by using the same scale for the different projectiles. All the BSB curves exhibit noticeable superimposed bulges in the high electron energy region. These superimposed structures are originated by emission from partially occupied SESs, whose partial contributions are also displayed in the figure for H^{+} and He^{+} projectiles. For all the projectiles the SES emission is confined to the same final energy range, which is determined by the parallel momentum conservation given by the delta function of Eq. (1). As discussed in Ref. [27], the remarkable SES contribution to the electron emission spectrum is due to the fact that the SESs of Cu(111) present highly peaked electron densities near the surface, which favors the electron ejection from such states when the projectile moves far from the surface plane, where the contribution from other initial states becomes small [26]. As shown in Fig. 2, the SESs give rise to the highest contribution to the total ground state electron density in the selvedge region. But the relative importance of the SES contribution decreases for the heavier projectiles. This is easily understood if we take into account that the SES contribution is more relevant when the projectile runs at a certain distance from the last atomic layer, where differences between the electronic density associated with the SES and those corresponding to other occupied electronic states are larger [26, 27]. Larger masses allow ions to reach closer distances to the surface, inducing a strong electron emission also from different occupied electronic states. Hence, the electron emission probability increases while the SES effect diminishes as the projectile mass augments. In other words, when projectiles move far away from the surface plane, only SES electrons are strongly affected by the external perturbation,

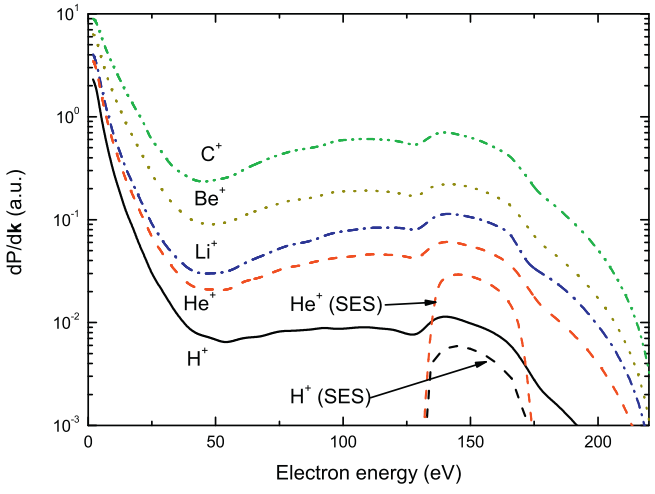

Fig. 1. Differential probability of electron emission from the valence band, as a function of the electron energy, for the emission angle $\theta_e = 30$ °. Comparison between results for different simply charged ions impinging with velocity $v = 2$ a.u. on a Cu(111) surface with the glancing angle $\alpha = 0.1$ °. Also SESs contributions for H^{+} and He^{+} ions are displayed.

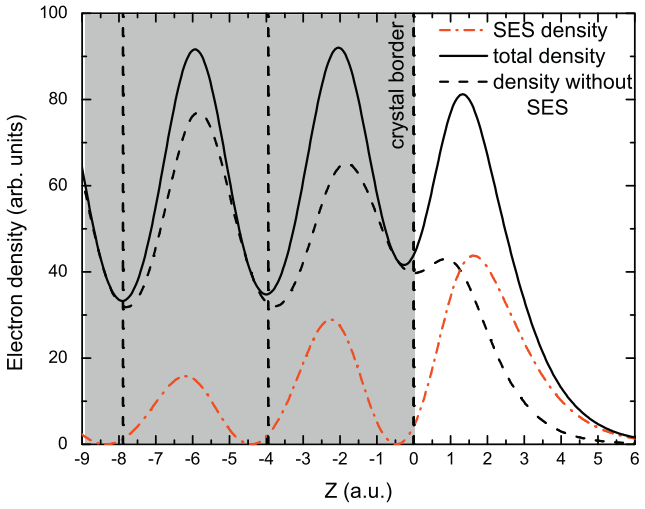

Fig. 2. Total ground state electron density ($|\phi(z)|^2$) in the region close to the topmost layer and the relative contribution from the SESs for a Cu(111) surface.

giving rise to a remarkable SES contribution. But when the distance of the closest approach diminishes keeping the velocity as a constant, the SES structure becomes smaller, producing only a smooth shoulder in the electron emission spectrum.

We have also studied the effect of the total charge for different ionic projectiles. Fig. 3 shows $dP_{vb}/d\mathbf{k}_f$ normalized by the square of the total projectile charge q, as a function of the electron energy, for C^{+q}, Be^{+q} and Li^{+q} with $q = 1, 2, 3$. The curves present similar features for all

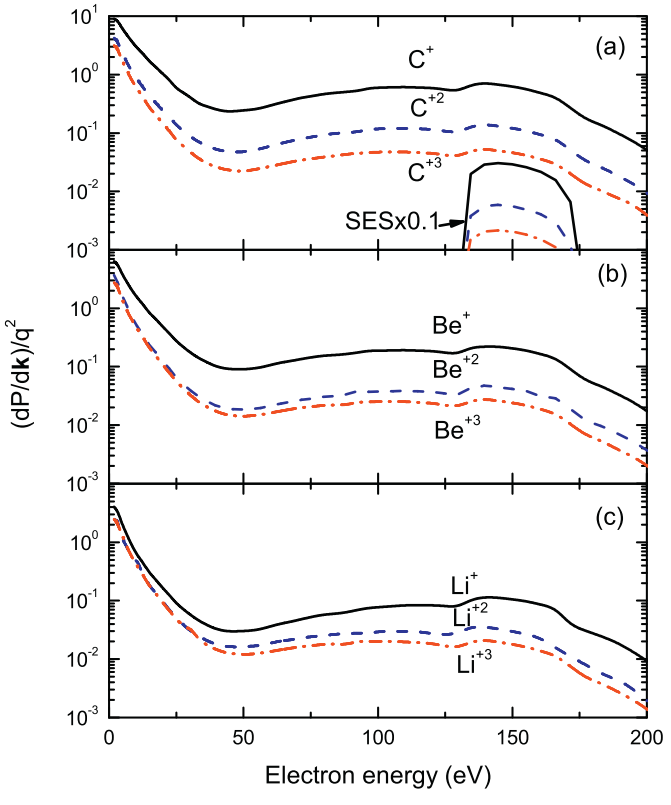

Fig. 3. Differential probability of electron emission from the valence band, normalized by the square of the charge state q, for the emission angle $\theta_e = 30$ °, as a function of the electron energy. The following ions impinging with velocity $v = 2$ a.u. on a Cu(111) surface, with the glancing angle $\alpha = 0.1$°, are considered: a) C^{+q}, b) Be^{+q}, c) Li^{+q} with $q = 1, 2, 3$. Also SESs contributions (multiplied by 0.1) for C^{+q} projectiles are displayed in the panel a).

the ions: the normalized emission probability decreases when q increases, being the SES structures slightly more pronounced for the lower charge states. This effect is again related to the projectile trajectory that makes that the relative importance of the SES contribution slightly augments for single charge projectiles, as shown in the case of carbon ions. The same behavior was observed for different emission angles in the scattering plane as well as outside it. To analyze this trajectory effect in more detail, in Fig. 4 we show the outgoing projectile paths for the different ions of Fig. 3. In all the cases we observe that as a result of the attractive action of the induced potential, the closest distance to the surface decreases when q augments. But at the same time, the path length that the ion remains moving in the selvage region of the metal diminishes as the charge state increases. Consequently, for increasing ionic charges the q^2-normalized emission probability decreases and simultaneously, the SES contribution becomes less relevant. However, the question that still remains is whether the variation of the relative weight of the SES contribution with the projectile charge state is entirely caused by the different distances of approach of the trajectories.

In order to find out if the influence of the charge state of the projectile on the emission probability can be explained by differences among trajectories only, we eliminated this effect choosing arbitrarily the H^+ trajectory for the different ions. In Fig. 5 we plot electron emission spectra for different carbon ions, considering two ejection angles in the scattering plane: $\theta_e = 30\,^\circ$ and $\theta_e = 60\,^\circ$. We observe that for both emission angles when identical trajectories are considered, the charge state of the projectile affects the low electron energy region of the spectrum, while the higher energy region, where the SES structure appears, remains unchanged for the different ionic charges. This behavior can be explained taking into account the important role of the structure charge $\tilde{Z}_P(\mathbf{Q})$, whose value varies from q for low transferred momenta to almost Z_P for high Q values. Then, for different ionic projectiles with the same nuclear charge $Z_P = 6$, differences in the electron distributions arise in the low electron energy region, which is associated with low Q values, where the structure charge $\tilde{Z}_P(\mathbf{Q})$ tends to the charge state q.

Similarly, the influence of the atomic number of the projectile on the emission probability cannot be only explained by differences among

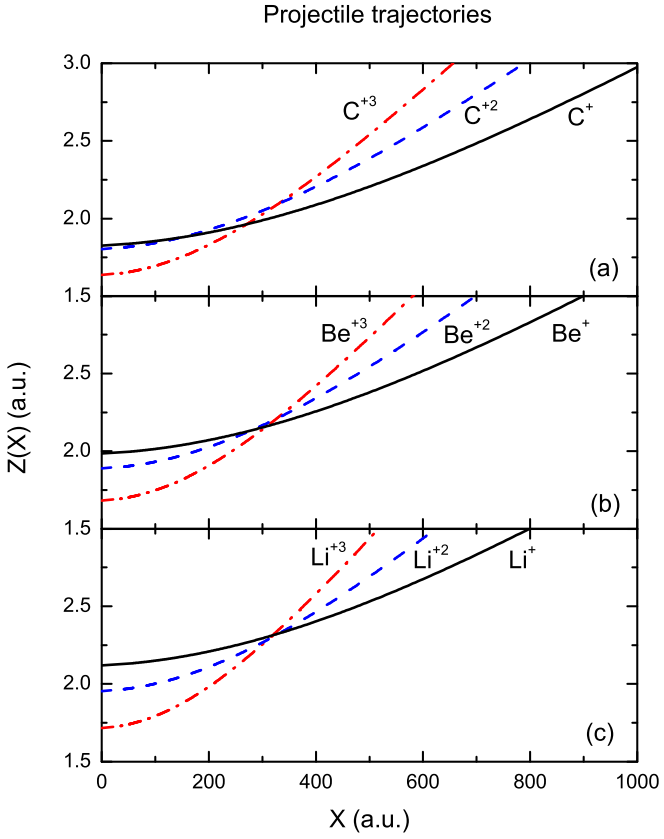

Fig. 4. Distance to the surface $Z(X)$, as a function of the coordinate X along the incidence direction on the surface plane, for the outgoing projectile paths corresponding to the cases of Fig. 3.

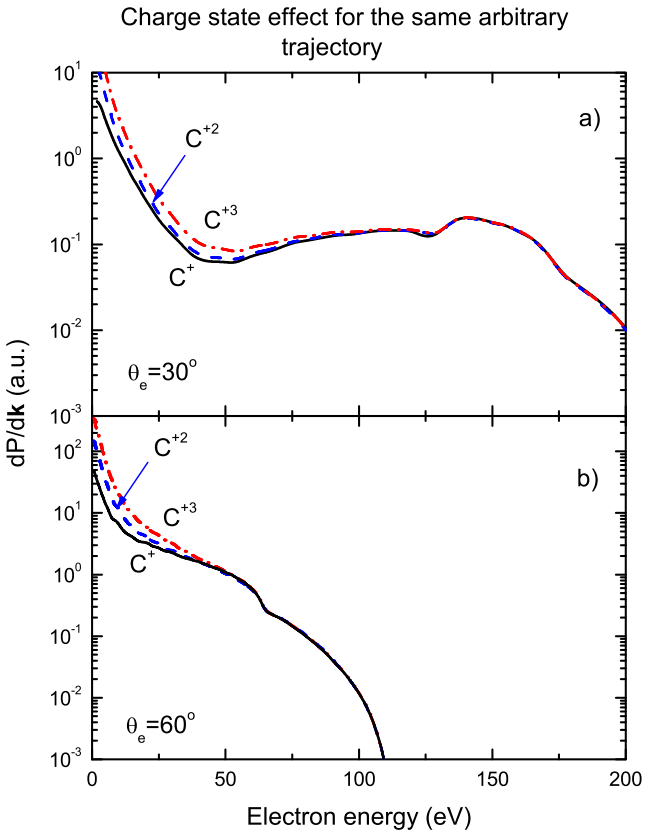

Fig. 5. Influence of the projectile charge state on electron emission spectra. Comparison between differential electron emission probabilities for C^+, C^{+2} and C^{+3}, for the emission angles: a) $\theta_e = 30\,^\circ$ and b) $\theta_e = 60\,^\circ$. All the projectiles following the same arbitrary trajectory, as explained in the text.

Similarly, the influence of the atomic number of the projectile on the emission probability cannot be only explained by differences among

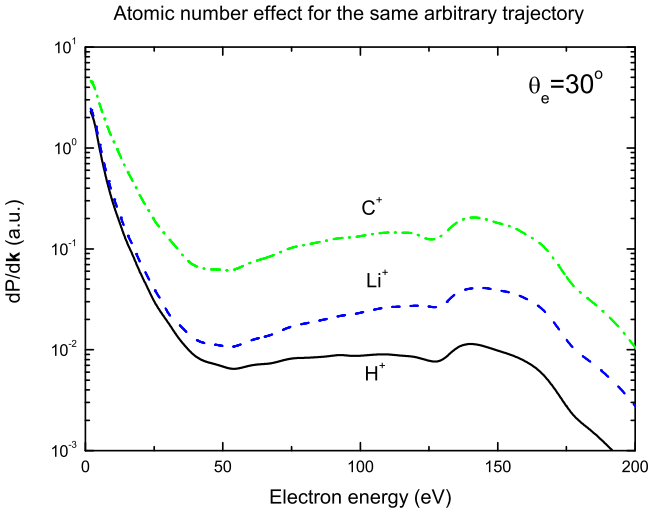

Fig. 6. Influence of the projectile atomic number Z_P on electron emission spectra. Comparison between differential electron emission probabilities for C^+, Li^+ and H^+ for the emission angle $\theta_e = 30\,^\circ$. All the projectiles following the same arbitrary trajectory, like in Fig. 5.

closest approach distances. From Fig. 6, electron emission probabilities for H^+, Li^+ and C^+ projectiles, all of them evaluated using the proper H^+ trajectory, are rather similar at low electron energies, but differences increase as the electron energy augments. Thus, for simply charged ions with different atomic numbers, higher atomic numbers induce higher emission probabilities at high electron energies, reducing consequently the importance of the SES contribution.

Finally, we point out that even though for the considered incidence conditions and projectiles, the electron excitation from the valence band is expected to be the main mechanism of electron emission from Cu(111), other processes associated with projectile neutralization or inner shell emission from target atoms might partially obscure the SES structure in the electron spectrum.

4. Conclusions

Electron emission spectra produced by grazing incidence of different dressed projectiles on a Cu(111) surface have been studied in the intermediate energy range. Like in the case of bare projectiles [26, 27], noticeable structures due to the presence of partially occupied SESs arise in the double differential electron distributions. Such structures are related to the high localization of the electronic density of the SESs around the selvage region, which promotes the electron emission process for projectiles moving outside the solid. Two important aspects are responsible for the behavior observed in the emission probability for different ionic projectiles — the trajectory and the projectile electron configuration — which play different and complementary roles. The effect of the trajectory for charged ions is similar to that observed for bare protons, i.e., when the distance of approach to the surface diminishes, the relative importance of the SES contribution becomes smaller, producing only a smooth shoulder in the electron emission spectrum. However, the SES effect also depends on the atomic number Z_P and the charge state q of the projectile, both parameters involved in the calculus of the structure charge $Z_P(\mathbf{Q})$. Therefore, we conclude that not only the trajectory but also the electronic configuration of the projectile plays an important role in effects related to the SES excitation.

Acknowledgments

This work was partially supported by the Consejo Nacional de Investigaciones Cientficas y Técnicas (CONICET) (PIP 100332/2011), the Agencia Nacional de Promoción Científica y Tecnológica (PICT 2010-1084) and the Universidad Nacional de Buenos Aires, Argentina. V. M. S. (UBACYT 100691/2011) acknowledges the partial support from the University of the Basque Country (Grants No. IT-366-07 and No. IT-756-13) and the Spanish Ministry of Economy and Competitiveness MINECO (Grant No. FIS2013-48286-C2-1-P).

References

[1] A. Arnau, F. Aumayr, P.M. Echenique, M. Grether, W. Heiland, J. Limburg, R. Morgenstern, P. Roncin, S. Schippers, R. Schuch, N. Stolterfoht, P. Varga, T.J.M. Zouros, H.P. Winter, Surf. Sci. Rep. 27 (1997) 117.
[2] C. Burgdörfer, K. Lemell, B. Schiessl, C. Solleder, K. Reinhold, L. Tokési, in: P.D. Fainstein, M.A.P. Lima, J.E. Miraglia, E.C. Montenegro, R.D. Rivarola (Eds.), Wirtz, Proceedings of the XXIV International Conference on Photonic, Electronic and Atomic Collisions, World Scientific Publishing Co. Pte. Ltd 2006, p. 16.
[3] N. Nieuwjaer, C. Bénazeth, P. Benoit-Cattin, P. Cafarelli, M. Richard-Viard, Nucl. Inst. Methods Phys. Res. B 230 (2005) 317.
[4] S. Wethekam, H. Winter, D. Valdés, R.C. Monreal, Phys. Rev. B 79 (2009) 195408.
[5] S. Wethekam, G. Adamov, H. Winter, Nucl. Inst. Methods Phys. Res. B 230 (2005) 305.
[6] M. Richard-Viard, C. Bénazeth, P. Benoit-Cattin, P. Cafarelli, N. Nieuwjaer, Phys. Rev. B 76 (2007) 045432.
[7] F.W. Meyer, L. Folkerts, S. Schippers, Nucl. Inst. Methods Phys. Res. B 100 (1995) 366.
[8] A.G. Borisov, A. Mertens, S. Wethekam, H. Winter, Phys. Rev. A 68 (2003) 012901.
[9] N.V. Novikov, Ya.A. Teplova, V.V. Bondurko, Nucl. Inst. Methods Phys. Res. B 256 (2007) 21.
[10] Z.Y. Song, Z.H. Yang, G.Q. Xiao, Q.M. Xu, J. Chen, B. Yang, Z.R. Yang, Eur. Phys. J. D 64 (2011) 197.
[11] H.P. Winter, M. Vana, C. Lemell, F. Aumayr, Nucl. Inst. Methods Phys. Res. B 115 (1996) 224.
[12] X. Luo, B. Hu, Ch. Zhang, J. Wang, Ch. Chen, Phys. Rev. A 81 (2010) 052902.
[13] J.E. Miraglia, Phys. Rev. A 50 (1994) 2410.
[14] M.S. Gravielle, J.E. Miraglia, Phys. Rev. A 50 (1994) 2425.
[15] B. Obreshkov, U. Thumm, Phys. Rev. A 74 (2006) 012901.
[16] D. Goebl, Diego Valdés, E. Abad, R.C. Monreal, D. Primetzhofer, P. Bauer, Phys. Rev. B 84 (2011) 165428.
[17] A. Sindona, S.A. Rudi, S. Maletta, R.A. Baragiola, G. Falcone, P. Riccardi, Surf. Sci. 601 (2007) 1205.
[18] M. Pisarra, P. Ricardi, A. Cupolillo, A. Sindona, L.S. Caputi, Nanosci. Nanotechnol. Lett. 4 (2012) 1100.
[19] A. Sindona, M. Pisarra, S. Maletta, P. Riccardi, A. Cupolillo, G. Falcone, Nucl. Inst. Methods Phys. Res. B 269 (2011) 938.
[20] T. Hecht, H. Winter, A.G. Borisov, J.P. Gauyacq, A.K. Kazansky, Phys. Rev. Lett. 84 (2000) 2517.
[21] T. Hecht, H. Winter, A.G. Borisov, J.P. Gauyacq, A.K. Kazansky, Faraday Discuss. 117 (2000) 27.
[23] M. Alducin, V.M. Silkin, J.I. Juaristi, E.V. Chulkov, Phys. Rev. A 67 (2003) 032903.
[24] V.M. Silkin, J.M. Pitarke, E.V. Chulkov, P.M. Echenique, Phys. Rev. B 72 (2005) 115435.
[25] V.M. Silkin, M. Alducin, J.I. Juaristi, E.V. Chulkov, P.M. Echenique, J. Phys. Condens. Matter 20 (2007) 304209.
[26] C.D. Archubi, M.S. Gravielle, V.M. Silkin, Phys. Rev. A 84 (2011) 012901.
[27] C.D. Archubi, M. Faraggi, M.S. Gravielle, V.M. Silkin, Phys. Rev. B 89 (2014) 155421.
[28] E.V. Chulkov, V.M. Silkin, P.M. Echenique, Surf. Sci. 391 (1997) L1217; Surf. Sci. 437 (1999) 330.
[29] M.N. Faraggi, M.S. Gravielle, V.M. Silkin, Phys. Rev. A 69 (2004) 042901.
[30] M.N. Faraggi, M.S. Gravielle, M. Alducin, J.I. Juaristi, V.M. Silkin, Phys. Rev. A 72 (2005) 012901.
[31] C.A. Ros Rubiano, M.S. Gravielle, D.M. Mitnik, V.M. Silkin, Phys. Rev. A 85 (2012) 043422.
[32] I. Aldazabal, M.S. Gravielle, J.E. Miraglia, A. Arnau, V.H. Ponce, Nucl. Inst. Methods Phys. Res. B 232 (2002) 53.
[33] E. Clementi, C. Roetti, At. Data Nucl. Data Tables 14 (177) (1974) 237.
[34] M.S. Gravielle, Phys. Rev. A 58 (1998) 4622.
[35] J.F. Ziegler, J.P. Biersack, U. Littmark, The Stopping and Range of Ions in Solids, vol. 1, Pergamon Press, New York, 1985.
[36] J. Seifert, A. Schüller, H. Winter, R. Wlodarczyk, J. Sauer, M. Sierka, Phys. Rev. B 82 (2010) 035436.